Journal of Alloys and Compounds 480 (2009) 737–740

Contents lists available at ScienceDirect

Journal of Alloys and Compounds

journal homepage: www.elsevier.com/locate/jallcom

Investigation of structural and magnetic properties of nanocrystalline $Ni_{0.3}Zn_{0.7}Fe_2O_4$ prepared by high energy ball milling

M. Jalaly, M.H. Enayati*, F. Karimzadeh

Department of Materials Engineering, Isfahan University of Technology, Isfahan 84156-83111, Iran

ARTICLE INFO

Article history:
Received 1 December 2008
Received in revised form 9 February 2009
Accepted 10 February 2009
Available online 23 February 2009

Keywords:
Nanostructured materials
Magnetically ordered materials
Mechanical alloying
Spin dynamics

ABSTRACT

High energy ball milling was used to produce nanocrystalline $Ni_{0.3}Zn_{0.7}Fe_2O_4$ ferrite from stoichiometric mixture of ZnO, NiO, Fe_2O_3 powders. The structural, chemical and magnetic properties of Ni–Zn ferrite was determined by X-ray powder diffractometry (XRD), scanning electron microscopy (SEM), Fourier transmission infrared spectroscopy (FTIR), vibrating sample magnetometer (VSM) and ac susceptometer measurements. The mechanism of formation this ferrite was appeared to engage two steps: diffusion of ZnO in Fe_2O_3 and formation of Zn ferrite followed by diffusion of NiO in Zn ferrite and formation of Ni–Zn ferrite. The crystallite size of final product after 60 h ball milling was estimated to be about 18 nm which increased to 30 nm after annealing at 800 °C for 4 h. The VSM results indicated that the magnetization did not saturate and coercivity and remanence were zero. The dynamic properties of 60 h ball milled sample were investigated by ac susceptibility using the Neel–Brown, Vogel–Fulcher and power laws for superparamagnetism/spin glass. The frequency-dependence of blocking temperature can be well described by the Vogel–Fulcher law, and fitting the experimental data with Neel–Brown model and power law give unphysical value for relaxation time.

© 2009 Published by Elsevier B.V.

1. Introduction

The nanocrystalline materials have optimum magnetic properties relative to conventional materials. It is well known that the microstructure, especially the crystallite size, essentially determines the hysteresis loop of the soft ferromagnetic materials [1].

Ni–Zn ferrite is a soft magnetic material and has the spinel structure in which metallic cations Fe^{3+}/Zn^{2+} occupy the tetrahedral sites while Fe^{3+}/Ni^{2+} occupy the octahedral sites [2]. Nanocrystalline Ni–Zn ferrite has the extensive applications such as recording heads, antenna rods, loading coils, microwave devices, core material for power transformers in electronics and telecommunication applications due to its improved magnetic behavior and high resistivity and low eddy current losses [3,4]. Because of the reduction of crystallite size (or particle size) to a few nanometers, nanocrystalline soft ferrites exhibit high coercivities and low saturation magnetization [5]. In particular, nanosized mixed ferrites containing zinc have attracted considerable attention. Dasgupta et al. synthesized different composition of Mn–Zn ferrite by mechanochemical method and studied the structural and dynamic magnetic properties of ferrite [6]. Ounnunkad et al. produced the Mg–Zn ferrite by conventional thermal solid state reaction and investigated the variation of static magnetic properties with Zn content [7]. Gözüak et al. also synthesized the Co–Zn ferrite via polyethylene glycol (PEG)-assisted hydrothermal route and characterized its structural and magnetic properties [8].

Ni–Zn ferrite can be synthesized by various methods including mechanical alloying. It is well known that the milling parameters can significantly influence the structural evolution during mechanical alloying [9–13]. It is also reported that the physical properties of Ni–Zn ferrite are very sensitive to the methods of preparation. Bid and Pradhan [14] synthesized nanocrystalline $Ni_{0.5}Zn_{0.5}Fe_2O_4$ after 11 h ball milling with a ball-to-powder mass ratio of 40:1. They found that NiO has a slower diffusion in Fe_2O_3 lattice than ZnO.

It is found that when the particle diameter reduced to a definite size, spinel nanoparticles may exhibit the so-called superparamagnetic behavior, which is of great interest in macroscopic quantum tunneling of spin states [15]. When nanoparticle size is smaller than the superparamagnetic critical size, above the blocking temperature, the hysteresis behavior vanishes and the magnetization direction of the particles simply follows the direction of the applied magnetic field. For the $Ni_{0.8}Co_{0.2}Fe_2O_4$ ferrite, the superparamagnetic behavior was observed and attributed to the size of equiaxial shaped nanoparticles below the superparamagnetic critical size [16]. The dynamics of magnetic behavior of nanosized particles have been interested over the last few years. Various phenomenological laws are generally used for explanation of magnetic dynamic behav-

* Corresponding author. Fax: +98 311 3912752.
E-mail address: ena78@cc.iut.ac.ir (M.H. Enayati).

0925-8388/$ – see front matter © 2009 Published by Elsevier B.V.
doi:10.1016/j.jallcom.2009.02.042

ior. The exponentially Neel–Brown theory predicts the relaxation time for weakly interacting superparamagnetic systems [17,18]. In assemblies with considerable dipole–dipole or exchange interactions, the magnetic relaxation has been explained by Vogel–Fulcher (VG) law [19], which is a modification of the Neel–Brown theory. A power law has been also used to describe the spin-glass behavior [20].

The goal of this work was to investigate the structural and magnetic properties of nanocrystalline $Ni_{0.3}Zn_{0.7}Fe_2O_4$ prepared by high energy ball milling of initial oxide powders.

2. Experimental

Fe_2O_3 (300–500 nm), ZnO (100–200 nm) and NiO (50–150 nm) powders with purity 99% supplied by Merck were used as the starting materials with molar ratio of 1:0.7:0.3. $Ni_{0.3}Zn_{0.7}Fe_2O_4$ ferrite was synthesized from these powders by high energy ball milling. The blend of powders was hand-ground in air using an agate mortar to obtain a homogeneous mixture of raw powders. Ball milling of powder mixture was conducted in a planetary ball mill at 600 rpm under air atmosphere up to 60 h using a ball-to-powder mass ratio of 10:1. The milling vial (125 ml) and balls (20 mm) were hardened chromium steel. Isothermal annealing of powders was carried out at 800 °C for 4 h under air to eliminate the milling induced crystal strain and defects. The heating rate up to 800 °C was 10 °C/min and the samples were cooled in air. The structural and phase composition of samples were investigated by X-ray powder diffraction (XRD) analysis at room temperature in a Philips X'Pert diffractometer (40 kV) using Cu Kα radiation ($\lambda = 0.15406$ nm). The crystallite size and internal strain of samples were estimated by broadening analysis of XRD peaks using Williamson–Hall formula [21]:

$$\frac{\beta}{2}\cot\theta = \frac{0.45\lambda}{\sin\theta D} + \varepsilon \quad (1)$$

where β is the full width at half maximum (FWHM) of the XRD peaks, θ is the Bragg angle, λ is the X-ray wave length, D is the crystallite size and ε is the value of internal strain. In this method, $\beta\cot\theta/2$ is plotted against $0.45\lambda/\sin\theta$. Using a linear fitting to this plot, the intercept gives the strain (ε) and the slope gives the particle size ($1/D$). Infrared spectroscopic analysis, with KBr pellet method, was carried out at the range of 350–2000 cm^{-1} using a Jasco FTIR300E Fourier Transform InfraRed spectrometer. The hysteresis loops of samples were measured at room temperature by using of vibrating sample magnetometer (VSM). The ac susceptibility measurements were performed using a Lake Shore Ac Susceptometer (Model 7000).

3. Results and discussion

3.1. Structural aspects

Fig. 1 shows the XRD patterns of NiO, ZnO and Fe_2O_3 powder mixture as-received and after different ball milling times. The pattern of as-received powder mixture includes only the sharp peaks of initial oxide phases. It is evident that the XRD peaks of initial oxides were broadened and their intensities reduced during ball milling. After 20 h ball milling, $Ni_{0.3}Zn_{0.7}Fe_2O_4$ phase was formed as noticed by appearance of (2 2 0) characteristic peak at $2\theta \sim 30^\circ$. The XRD peaks of oxides gradually disappeared with increasing ball milling time and the fraction of Ni–Zn ferrite was increased. The

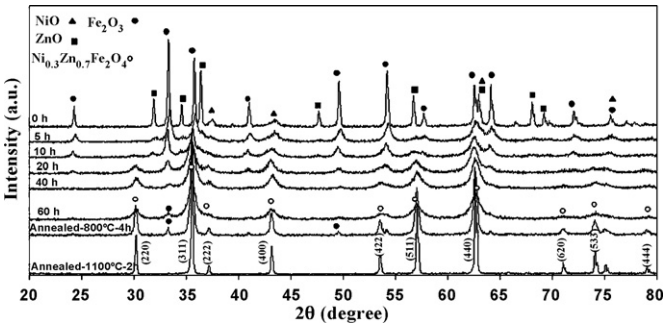

Fig. 1. X-ray patterns of as-mixed oxides, as-milled $Ni_{0.3}Zn_{0.7}Fe_2O_4$ and annealed samples.

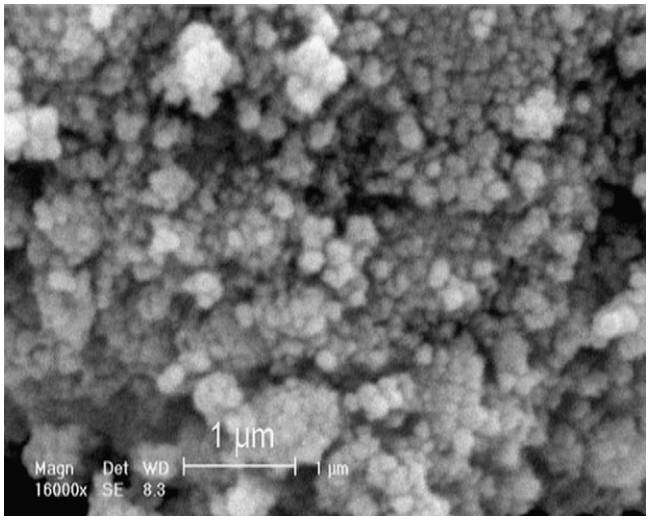

Fig. 2. SEM micrograph of ball milled (60 h) Ni–Zn ferrite nanoparticles.

formation of $Ni_{0.3}Zn_{0.7}Fe_2O_4$ occurs by reaction (2):

$$Fe_2O_3 + 0.3NiO + 0.7ZnO \rightarrow Ni_{0.3}Zn_{0.7}Fe_2O_4 \quad (2)$$

After 60 h ball milling, the XRD peaks of sample mostly include the Ni–Zn ferrite phase, although a slight amount of Fe_2O_3 phase are still evident. The XRD results in Fig. 1 show that the ZnO phase are first vanished during ball milling, indicating that the rate of dissolution of ZnO in Fe_2O_3 lattice is faster than that of NiO. Similar behavior is reported by Bid and Pradhan [14] for Ni–Zn ferrite and Zheng et al. [22] for Mn–Zn ferrite. The mechanism of formation of Ni–Zn ferrite can be therefore suggested to include two stages, as follows:

$$ZnO + Fe_2O_3 \rightarrow ZnFe_2O_4 \quad (3)$$

$$NiO + ZnFe_2O_4 + Fe_2O_3 \rightarrow NiZnFe_2O_4 \quad (4)$$

In first stage ZnO diffuses in Fe_2O_3 forming Zn ferrite. Then NiO gradually diffuse in Zn ferrite to produce Ni–Zn ferrite structure. The crystallite size of $Ni_{0.3}Zn_{0.7}Fe_2O_4$ after 60 h ball milling was determined to be about 18 nm.

In order to eliminate internal lattice strain and reduce density of crystal lattice defects, annealing process was carried out at 800 °C for 4 h in air. The XRD peaks of annealed samples are shown in Fig. 1. The intensity of peaks increased after annealing due to crystallite growth and reduction of internal strain. The crystallite size after annealing was increased to 30 nm. It should be noted that a slight amount of Fe_2O_3 was present on XRD pattern after annealing at 800 °C for 4 h. However, the remaining Fe_2O_3 was disappeared by annealing at 1100 °C for 2 h. In this case, the crystallite size of Ni–Zn ferrite increased to about 1 μm.

SEM micrograph of powder particles after 60 h ball milling is shown in Fig. 2. The sample has an agglomerated morphology consists of nanosized spherical particles with a narrow distribution of 50–150 nm.

Fig. 3 shows the room temperature IR spectra of the as-mixed oxides as well as ball milled (60 h) $Ni_{0.3}Zn_{0.7}Fe_2O_4$ in the range of 350–2000 cm^{-1}. The reflection of IR spectra corresponding to as-received powder is seen in Fig. 3(a). The bands of oxides are located at around of 500 cm^{-1}. On the curve (a), the observed absorption bands below 700 cm^{-1} belong to stretching vibration of Fe–O [23], Zn–O [24] and Ni–O [25]. The absorption bands around ~1640 and 1380 cm^{-1} can be attributed to adsorbed water and hydrocarbon impurity of powders, respectively. As can be seen in Fig. 3(b), two characteristic bands at around 420 and 590 cm^{-1} are appeared after

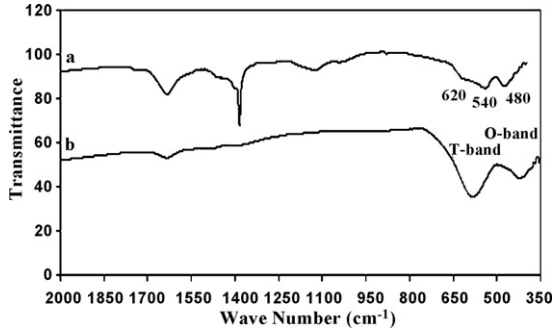

Fig. 3. FTIR spectra of (a) as-mixed oxides and (b) ball milled (60 h) Ni–Zn ferrite powders.

formation of ferrite, which are assigned as O and T bands, respectively. In general, all ferrites with spinel structure show these two typical absorption bands. According to Waldron [26], the ferrites can be considered as continuously bonded crystals. Since the ferrites have two sublattices (tetrahedral and octahedral groups), the T-band is associated to intrinsic vibrations of tetrahedral groups (Zn^{2+} ions) and O-band to the octahedral groups (Ni^{2+} ions).

The ball milled Ni–Zn ferrite has a conventional structure similar to the structure of various ferrites prepared by different methods. The XRD and IR results confirmed that nanocrystalline Ni–Zn ferrite had a spinel structure. This structure includes tetrahedral and octahedral sites which can be occupied by metallic ions such as Ni^{2+}, Zn^{2+} and Fe^{3+}.

3.2. Magnetic properties

Magnetization measurements of the prepared samples were carried out using a vibrating sample magnetometer (VSM) at room temperature. Fig. 4 shows the hysteresis loop of ball milled (60 h) and annealed (800 °C, 4 h) $Ni_{0.3}Zn_{0.7}Fe_2O_4$. As can be seen, the samples did not attain to the saturated magnetization state at high applied magnetic field of 1.5 T. The zero remanence and coercivity and non-saturated magnetization obviously show a typical superparamagnetic behavior without hysteresis, which is attributed to the equiaxial shaped nanoparticles which have a size smaller than the superparamagnetic critical size. The relative low value of magnetization in as-milled sample is due to the very small crystallite size, the remaining initial oxides, and lattice defects and strains induced during milling. The strains in fine particles produced by ball milling affect the overall magnetization (probably due to an increase in surface spins) because of displacement of ions and

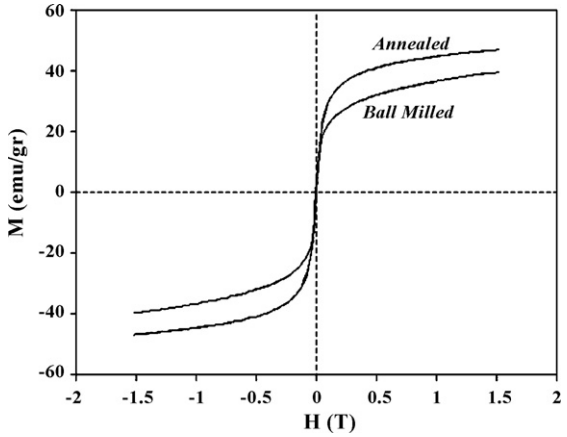

Fig. 4. Magnetic hysteresis loops of ball milled (60 h) and annealed (800 °C, 4 h) Ni–Zn ferrite.

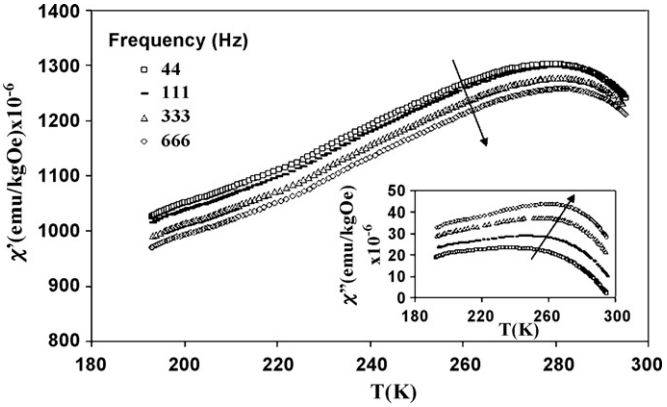

Fig. 5. Temperature dependence of the real part of ac susceptibility for ball milled (60 h) nanoparticles at different frequencies. The data in inset are the imaginary part of ac susceptibility. The arrows indicate increasing frequencies.

disordering. After annealing, the magnetization is considerably increased as a result of lattice strain as well as crystal defects reduction in annealed powders.

In order to clarify the type of interactions between the nanoparticles, the magnetic dynamics of 60 h ball milled sample was investigated by real (χ') and imaginary (χ'') component of the ac susceptibility. Fig. 5 shows the variation of real part and imaginary part of ac susceptibility with temperature in an ac field of 10 Oe at frequencies of 44–666 Hz. As can be seen, all curves have same trends and exhibit a maximum at temperature of T_B for both χ' and χ'' which is the characterization of superparamagnetic behavior of blocking/freezing process. This peak shifts towards the higher temperature and its magnitude reduces with increasing frequency. There is a practical parameter, Φ, to identify the dynamic behavior of blocking/freezing process with a value of ~0.1–0.13 for superparamagnetic particles and ~0.005–0.05 for spin glass [27]. Φ was obtained using the data given in Fig. 5:

$$\Phi = \frac{\Delta T_B}{T_B \, \Delta \log_{10}(f)} \approx 0.005 \tag{5}$$

where ΔT_B is the difference between blocking temperatures, T_B, measured in the $\Delta\log_{10}(f)$ frequencies. The Φ value given by Eq. (5) probably exhibits the spin-glass behavior, although it is often difficult to experimentally distinguish between spin glass and superparamagnetic behavior [28].

There are several theories to interpret the superparamagnetic/spin-glass interactions. In the non-interacting superparamagnetic assemblies, the frequency-dependence of blocking temperature follows the Neel–Brown model:

$$\tau = \tau_0 \exp\left(\frac{E_A}{k_B T_B}\right) \tag{6}$$

in which, $\tau_0 = \rho N_0 h / 2K_{eff}A$ and $E_A = K_{eff}V$. In Eq. (6) E_A is the barrier energy, k_B the Boltzmann's constant, T_B the blocking temperature, ρ the density, N_0 the Avagadro's number, h the Plancks's constant, A the atomic weight, K_{eff} the magnetocrystalline anisotropy constant and V the particle volume. τ_0 is in the range 10^{-9} to 10^{-13} s for superparamagnetic particles [29] and $\tau = 1/f$ is related to measuring frequency. By fitting the experimental data in Fig. 5 to Eq. (6), we have found an unphysical value of $\sim 10^{-116}$ s for τ_0 (Fig. 6) which is much smaller than 10^{-13} s for superparamagnetic systems. This value indicates that there exist strong interactions among nanoparticles and Neel–Brown model cannot interpret this behavior. As mentioned earlier, the Vogel–Fulcher law describes the behavior

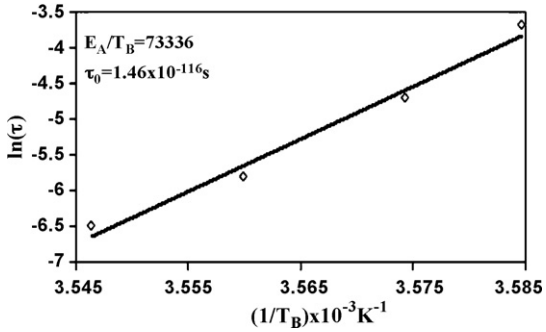

Fig. 6. The best fit of logarithm of measuring frequency as a function of reciprocal of the blocking temperature in terms of Neel–Brown model.

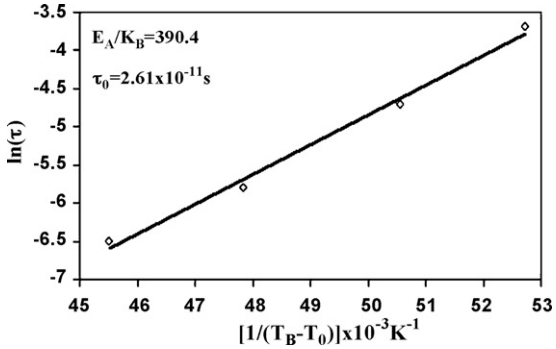

Fig. 7. The best fit of logarithm of measuring frequency as a function of reciprocal of the difference between the blocking temperature and T_0 in terms of Vogel–Fulcher law.

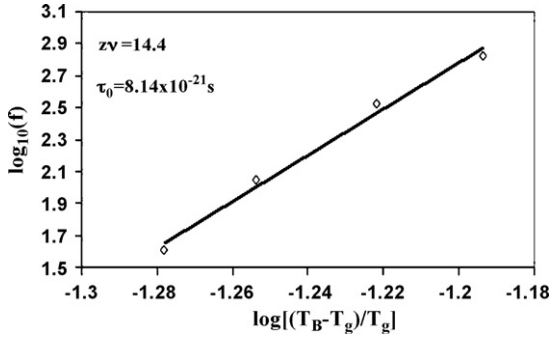

Fig. 8. The best fit of log–log plot of reduced temperature, ε, versus frequencies.

of magnetically interacting particles as follows:

$$\tau = \tau_0 \exp\left(\frac{E_A}{k_B(T_B - T_0)}\right) \quad (7)$$

Here T_0 is the effective temperature. Fig. 7 shows the fit of experimental data to Eq. (7) which gives: $\tau_0 = 2.61 \times 10^{-11}$ s, $E_A = 5.38 \times 10^{-14}$ erg and $T_0 = 260$ K. A good agreement of experimental data and Vogel–Fulcher law is observed suggesting that the phenomenon taking place at T_B is related to blocking of an ensemble of interacting nanoparticles rather than a collective freezing that occurs in a spin-glass system.

The possibility of spin-glass behavior was checked by the power equation of:

$$f = f_0 \varepsilon^{z\upsilon} \quad (8)$$

in which $\varepsilon = (T_B - T_g)/T_g$ is the reduced temperature, f is the frequency, z is the dynamic scaling exponent and υ is the correlation length scaling exponent. For spin-glass, typical values of $\tau_0 = 1/f_0$ calculated by Eq. (8), are within the range of 10^{-11} to 10^{-12} s [30]. Fig. 8 shows the log–log plot of reduced temperature versus applied frequencies (f). The obtained parameters are $\tau_0 = 8.14 \times 10^{-21}$ s, $z\upsilon = 14.4$ and $T_g = 265$ K. These values imply that spin-glass interaction does not exist in this system.

4. Conclusion

Nanocrystalline magnetic $Ni_{0.3}Zn_{0.7}Fe_2O_4$ ferrite was synthesized by high energy ball milling of initial blend of oxides and subsequent annealing. XRD results showed that the mechanism of formation of Ni–Zn ferrite involved two steps, the formation of Zn ferrite followed by the formation of Ni–Zn ferrite. The crystallite sizes of ball milled (60 h) and annealed (800 °C for 4 h) samples were calculated to be 18 and 30 nm, respectively. The non-saturated magnetization and zero remanence and coercivity was detected in hysteresis loop which was exhibited the superparamagnetic state. After annealing, the magnetization increased due to a reduction in density of lattice defects and strain. The dynamic behavior of nanoparticles is well described by the Vogel–Falcher law for interacting particles. The fitting of experimental data by Neel–Brown model and power law for spin-glass resulted in an unphysical values for relaxation time.

References

[1] I. Chicinas, J. Optoelectron. Adv. Mater. 8 (2006) 439–448.
[2] J.M. Daniels, A. Rosencwaig, Can. J. Phys. 48 (1970) 381–396.
[3] K. Kondo, T. Chiba, S. Yamada, J. Magn. Magn. Mater. 254–255 (2003) 541–543.
[4] D. Stoppels, J. Magn. Magn. Mater. 160 (1996) 323–328.
[5] W.C. Kim, S.L. Park, S.J. Kim, S.W. Lee, C.S. Kim, J. Appl. Phys. 87 (2000) 6241–6243.
[6] S. Dasgupta, K.B. Kim, J. Ellrich, J. Eckert, I. Manna, J. Alloys Compd. 424 (2006) 13–20.
[7] S. Ounnunkad, P. Winotai, S. Phanichphant, J. Electroceram. 16 (2006) 363–368.
[8] F. Gözüak, Y. Köseoğlua, A. Baykal, H. Kavas, J. Magn. Magn. Mater. (2009), doi:10.1016/j.jmmm.2009.01.008.
[9] I. Manna, P. Nandi, B. Bandyopadhyay, K. Ghoshray, A. Ghoshray, Acta Mater. 52 (2004) 4133.
[10] A.C.F.M. Costa, E. Tortella, M.R. Morelli, R.H.G.A. Kiminami, J. Magn. Magn. Mater. 256 (2003) 174–182.
[11] G. Nicoara, D. Fratiloiu, M. Nogues, J.L. Dormann, F. Vasiliu, Mater. Sci. Forum 235 (1997) 145–150.
[12] C. Suryanarayana, E. Ivanov, V.V. Boldyrev, Mater. Sci. Eng. 304–306A (2001) 151–158.
[13] B.S. Murty, S. Ranganathan, Int. Mater. Rev. 43 (1998) 101–134.
[14] S. Bid, S.K. Pradhan, Mater. Chem. Phys. 84 (2004) 291–301.
[15] C. Liu, B. Zhou, A.J. Rondinone, Z.J. Zhang, J. Am. Chem. Soc. 122 (2000) 6263–6267.
[16] J. Jiang, Mater. Lett. 61 (2007) 3239–3242.
[17] L. Neel, Ann. Geophys. 5 (1949) 99–136.
[18] W.F. Brown, Pyhs. Rev. 130 (1963) 1677–1686.
[19] S. Shtrikman, E.P. Wohlfarth, Phys. Lett. 85A (1981) 467–470.
[20] A.T. Ogielski, Phys. Rev. B 32 (1985) 7384–7398.
[21] K. Wiliamson, W.H. Hall, Acta Metall. 1 (1953) 22–31.
[22] Z.G. Zheng, X.C. Zhong, Y.H. Zhang, H.Y. Yu, D.C. Zeng, J. Alloys Compd. 466 (2008) 377–382.
[23] S. Mitra, S. Das, K. Mandal, S. Chaudhuri, Nanotechnology 18 (2007) 275608, doi:10.1088/0957-4484/18/27/275608.
[24] N. Lepot, M.K. Van Bael, H. Van den Rul, J. D'Haen, R. Peeters, D. Franco, J. Mullens, Mater. Lett. 61 (2007) 2624–2627.
[25] Y. Wang, J. Zhu, X. Yang, L. Lu, X. Wang, Thermochim. Acta 437 (2005) 106–109.
[26] R.D. Waldron, Phys. Rev. 99 (1955) 1727–1735.
[27] G.F. Goya, V. Sagredo, Phys. Rev. B 64 (2001) 235–241.
[28] A. Mydosh, Spin Glasses: An Experimental Introduction, Taylor and Francis, London, 1993.
[29] G.F. Goya, T.S. Berquo, F.C. Fonseca, M.P. Morales, J. Appl. Phys. 94 (2003) 3520–3528.
[30] B. Idzikowski, U.K. Robler, D. Eckert, K. Nenkov, K.H. Muller, Europhys. Lett. 45 (1999) 714–720.